Thickness-Dependent Refractive Index of 1L, 2L, and 3L MoS $_2$, MoSe $_2$, WS $_2$, and WSe $_2$

Hsu, Chunwei; Frisenda, Riccardo; Schmidt, Robert; Arora, Ashish; de Vasconcellos, Steffen Michaelis; Bratschitsch, Rudolf; van der Zant, Herre S.J.; Castellanos-Gomez, Andres

Important note
To cite this publication, please use the final published version (if applicable).
Please check the document version above.

COMMUNICATION

2D Materials

ADVANCED
OPTICAL
MATERIALS

www.advopticalmat.de

Thickness-Dependent Refractive Index of 1L, 2L, and 3L MoS$_2$, MoSe$_2$, WS$_2$, and WSe$_2$

Chunwei Hsu,* Riccardo Frisenda,* Robert Schmidt, Ashish Arora, Steffen Michaelis de Vasconcellos, Rudolf Bratschitsch, Herre S. J. van der Zant, and Andres Castellanos-Gomez*

An interesting aspect of 2D materials is the change of their electronic structure with the reduction of thickness. Molybdenum and tungsten-based transition metal dichalcogenides form an important family of 2D materials, whose members show a thickness-dependent bandgap and strong light–matter interaction. In this work, the experimental determination of the complex refractive index of 1-, 2-, 3-layer thick MoS$_2$, MoSe$_2$, WS$_2$, and WSe$_2$ in the range from 400 to 850 nm of the electromagnetic spectrum is reported by using microreflectance spectroscopy and combined with calculations based on the Fresnel equations. It is further provided a comparison with the bulk refractive index values reported in the literature and a discussion of the difference/similarity between our work and the monolayer refractive index available from the literature, finding that the results from different techniques are in good agreement.

Since the isolation of thin transition metal dichalcogenides (TMDCs) by mechanical exfoliation, Mo- and W-based dichalcogenides have attracted attention because of their thickness-dependent optical properties.[1] In particular, these materials display an indirect-to-direct bandgap transition when their thickness is reduced to a single layer, thereby significantly increasing

the photoluminescence quantum efficiency.[2–4] Moreover, the change of the band structure of these materials with thickness has been exploited in p–n junctions and in photodetectors whose spectral bandwidth can be controlled through the number of layers.[5–7] However, despite the interest aroused by these optical properties, a systematic study of the thickness-dependent complex refractive index $\tilde{n}$ on this family of materials is lacking.

In literature, there are two main schemes to investigate the complex refraction index of materials; they have both been applied to TMDCs. The first method is a Kramers–Kronig (KK) analysis of the reflection or transmission spectrum of the sample,[8] while in the second method, ellipsometry, the ellipticity induced in a linearly polarized beam reflected from the material surface is measured.[9–11] While the KK analysis has the advantage of being easy to implement experimentally, the method requires the knowledge of the full spectrum to calculate the KK relations. Approximations are thus needed to overcome the limited spectral range in experiments. Conversely, ellipsometry has the advantage of having high sensitivity, but its experimental implementation to probe micrometer samples is cumbersome. An additional third method (microreflectance) that we use in this work was first reported by Zhang and co-workers[12] for single-layer chemical vapor deposition- grown MoS$_2$. This technique, which is based on the analysis of the reflection of the material under investigation, is particularly well suited for the characterization of isotropic and anisotropic 2D and layered materials.[13–15]

Several reports have determined the dielectric function or refractive index for single-layer TMDCs[8–11] and their bulk counterparts[16,17] using these three techniques. By using ellipsometry, Shen and co-workers[10] reported the complex refractive index of single-layer MoS$_2$ in the region of the electromagnetic spectrum from near infrared (1600 nm) to near ultraviolet (200 nm). In the study by Li and co-workers,[8] Tony Heinz's group reported the complex dielectric function (related to the complex refractive index) of single-layer MoS$_2$, WS$_2$, MoSe$_2$, and WSe$_2$, extracted with the KK analysis of the reflectance spectra. In the study by Yu and co-workers,[18] ellipsometry measurements of the dielectric function of MoS$_2$ grown by chemical vapor deposition from one layer to multilayers were discussed. In this paper,

C. Hsu, Dr. R. Frisenda, Dr. A. Castellanos-Gomez
Materials Science Factory
Instituto de Ciencia de Materiales de Madrid (ICMM)
Consejo Superior de Investigaciones Científicas (CSIC)
Sor Juana Inés de la Cruz 3, 28049 Madrid, Spain
E-mail: riccardo.frisenda@csic.es; andres.castellanos@csic.es
C. Hsu, Prof. H. S. J. van der Zant
Kavli Institute of Nanoscience
Delft University of Technology
Delft 2600 GA, The Netherlands
E-mail: chunwei.hsu@mail.mcgill.ca
Dr. R. Schmidt, Dr. A. Arora, Dr. S. M. de Vasconcellos,
Prof. R. Bratschitsch
Institute of Physics and Center for Nanotechnology
University of Münster
48149 Münster, Germany

using the microreflectance method,[19] we determine the complex refractive index ($\tilde{n} = n - i \cdot \kappa$) in the 400–850 nm range of the spectrum for mechanically exfoliated 1, 2, and 3 layers of MoS_2, $MoSe_2$, WS_2, and WSe_2. The values of the complex refractive index were obtained by modelling the measured contrast between the TMDC flakes and SiO_2/Si substrates with different oxide thicknesses using Fresnel equations. We further compare our results with bulk and monolayer refractive index values available in the literature. Knowledge of the refractive index not only provides important insights for light–matter interaction in few-layer TMDCs, but also is a crucial starting point to optimize photonic and optoelectronic devices.[20]

Single-, bi-, and tri-layer (called 1L, 2L, and 3L, respectively, hereafter) TMDC flakes are fabricated by mechanical exfoliation of layered bulk TMDC crystals (see Experimental Section) with Nitto tape (SPV 224). The material cleaved with the tape is then transferred onto a Gelfilm substrate (from Gelpak, a commercially available polydimethylsiloxane substrate). **Figure 1**a is a transmission illumination mode optical microscopy image of an MoS_2 flake that contains 1L, 2L, and 3L regions deposited onto a Gelfilm substrate. In this ultrathin regime, the number of layers can be determined with high accuracy from microtransmittance or microreflectance measurements as the position and intensity of the excitons of MoS_2 monotonically depend on the number of layers.[2,4,21–25] Figure 1b shows the transmittance $T(E)$ spectra of the 1L, 2L, and 3L regions of the flake. The two resonances at 1.8 and 2.0 eV are the A and B excitons, which are separated in energy by the spin–orbit interaction.[19,25] The values of the transmittance confirm that the investigated regions are indeed single-, bi-, and tri-layer MoS_2.

An alternative method of quantifying the thickness of MoS_2 using the information from the transmittance is based on the quantitative analysis of the intensity (of the red, green, and blue channels) of the picture shown in Figure 1a.[26] Figure 1c shows three line profiles extracted from the blue channel intensity of the image in Figure 1a at the positions indicated by the solid lines. These line profiles reach the largest values in the PDMS region (with an intensity of approximately 180). However, in the flake region, their intensities decrease as the number of layers increases (165 for 1L, 145 for 2L, 129 for 3L). From these values, one can calculate the "blue channel" transmittance T_B of the flake by dividing the intensity of the flake with that of the substrate. We find in the 1L, 2L, and 3L a "blue channel" transmittance of 0.92, 0.81, and 0.71, respectively. Optical pictures of tens of different MoS_2 flakes were recorded and T_B of each flake was extracted. Figure 1d shows the T_B histogram built from 189 MoS_2 flakes. The histogram shows three peaks well separated from each other and centered around 0.88, 0.77, and 0.68 corresponding to 1L, 2L, and 3L, respectively.

Once the number of layers has been determined, the flakes are transferred onto SiO_2/Si substrates with different SiO_2 capping layers through an all-dry transfer technique.[27,28] The optical microscopy image of the MoS_2 flake (displayed in Figure 1a) transferred on a 69 nm SiO_2/Si substrate and recorded in epi-illumination mode is shown in Figure 1e. Importantly, the apparent color of the flakes depends both on the number of layers and on the SiO_2 thickness; see Figure 1f for examples of MoS_2 flakes deposited on Si substrates with different SiO_2 thicknesses. To determine the refractive index of the TMDCs, we measure their optical contrast and fit the
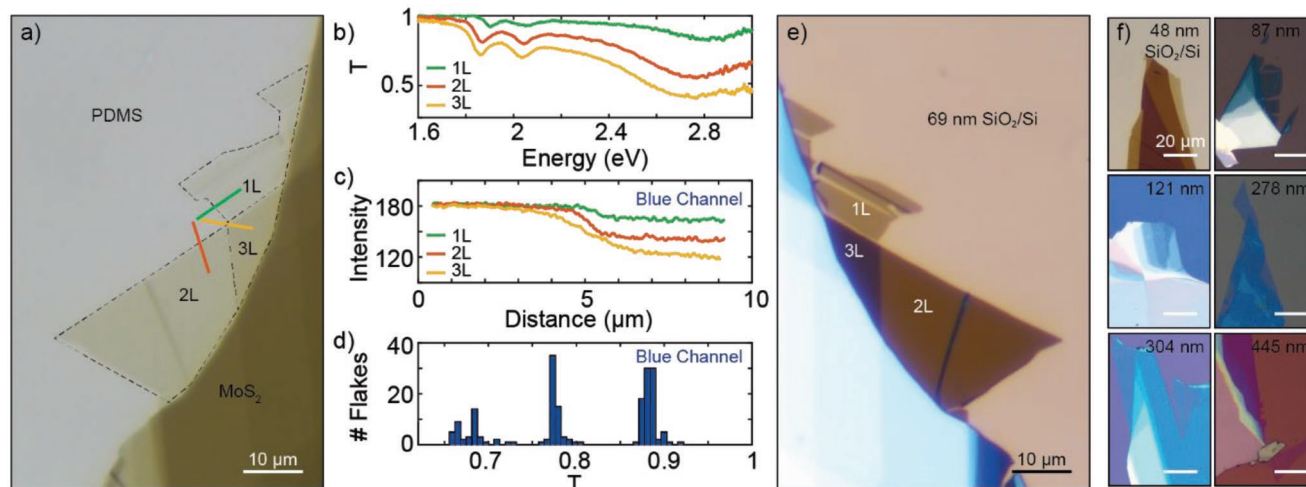

Figure 1. Optical microscopy of 1L, 2L, and 3L exfoliated MoS_2. a) Optical image of a mechanically exfoliated MoS_2 flake on a PDMS Gelfilm taken in transmission illumination mode optical microscopy. Dashed lines separate the 1L, 2L, and 3L regions of the MoS_2 flake. The three colored lines in the image correspond to the intensity profile in (c). b) Energy resolved transmittance of 1L, 2L, and 3L MoS_2. The dips at ≈1.8 and ≈2 eV in the spectra correspond to the A and B excitons, which are used to identify the thickness of the MoS_2 flake. c) The blue channel intensity line profile of 1L, 2L, 3L MoS_2 with the location shown in (a). From these three line profiles, the absorbance can be found and compared with the histogram in (c) to determine the number of layers. d) The histogram for the blue channel absorbance of the flakes. Here, the three peaks of 0.88, 0.77, and 0.68 correspond to the blue channel absorbance of 1L, 2L, and 3L MoS_2. e) Reflective mode optical images of the same MoS_2 flakes on 69 nm SiO_2/Si substrate after the dry-transfer. In the reflective mode optical microscopy, the contrast between the 1L, 2L, and 3L MoS_2 and the SiO_2/Si substrate is measured with a spectrometer. f) Reflective mode optical images of MoS_2 flakes on SiO_2/Si substrates with different thicknesses. A clear change of color is present among the different substrates, whose contrast with the flakes was used to calculate the complex refractive index.
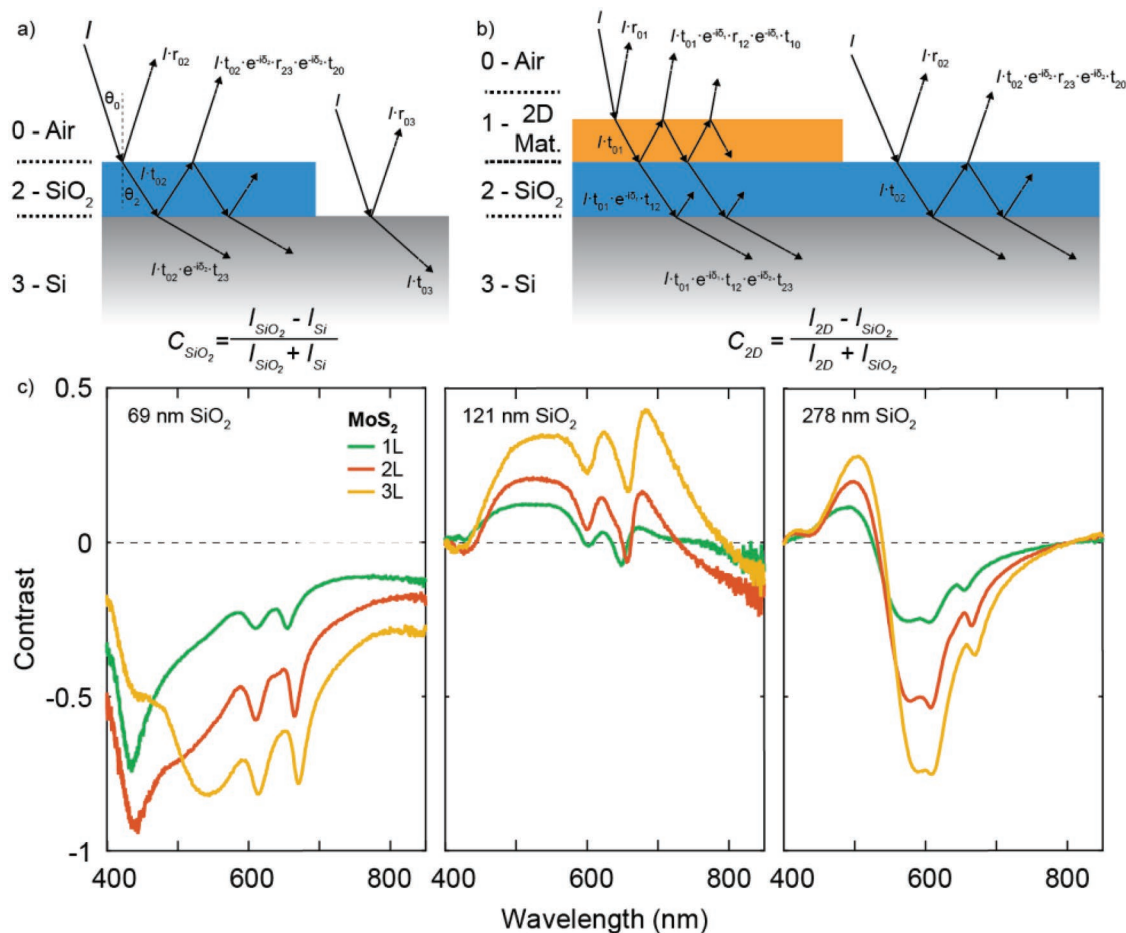
**ADVANCED
SCIENCE NEWS**

www.advancedsciencenews.com

**ADVANCED
OPTICAL
MATERIALS**

www.advopticalmat.de

Figure 2. Optical contrast of 1L, 2L, and 3L MoS$_2$ on different SiO$_2$/Si substrates. a) Schematic drawing of the three media system (air/SiO$_2$/Si) from which the thickness of SiO$_2$ can be determined. b) Schematic drawing of the four media system (air/TMDC/SiO$_2$/Si) from which the refractive index of a 2D material can be determined. c) Spectral contrast of MoS$_2$ on substrates with different SiO$_2$ thicknesses indicated as legends. The solid lines are the optical contrast measured for 1L, 2L, and 3L MoS$_2$ in the wavelength range of 400–850 nm.

resulting experimental data sets to a Fresnel law-based model that accounts for the reflections and refractions at each interface between different optical media (labeled hereafter as 0, 1, 2, and 3 for air, TMDC, SiO$_2$, and Si, respectively).[29] The layers corresponding to the TMDC and to the SiO$_2$ have thicknesses d_1 and d_2, respectively; see **Figure 2**a for a schematical drawing of the model.

When illuminating the system with light of intensity I_0 at normal incidence, the intensity of the light reflected from the substrate ($I_{\text{substrate}}$) can be calculated by summing all the optical beams going from medium 2 to medium 0 (see the sketch in Figure 2a):

$$I_{\text{substrate}} = I_0 \left| \frac{r_{02} + r_{23}e^{-2i\Phi_2}}{1 + r_{02}r_{23}e^{-2i\Phi_2}} \right|^2 \tag{1}$$

where $r_{ij} = (\tilde{n}_i - \tilde{n}_j)/(\tilde{n}_i + \tilde{n}_j)$ ($\tilde{n}_i$ is the complex refractive index of medium i) and $\Phi_2 = 2\pi n_2 d_2/\lambda$. When the TMDC is placed on the SiO$_2$/Si surface, the reflected intensity is modified as new reflections/refractions have to be considered (see the sketch in Figure 2b). The reflected intensity by the flake is now calculated as

$$I_{2D} = I_0 \left| \frac{r_{01}e^{i(\Phi_1+\Phi_2)} + r_{12}e^{-i(\Phi_1-\Phi_2)} + r_{23}e^{-i(\Phi_1+\Phi_2)} + r_{01}r_{12}r_{23}e^{i(\Phi_1-\Phi_2)}}{e^{i(\Phi_1+\Phi_2)} + r_{01}r_{12}e^{-i(\Phi_1-\Phi_2)} + r_{01}r_{23}e^{-i(\Phi_1+\Phi_2)} + r_{12}r_{23}e^{i(\Phi_1-\Phi_2)}} \right| \tag{2}$$

The optical contrast can be calculated by combining Equations (1) and (2):

$$C = \frac{I_{2D} - I_{\text{substrate}}}{I_{2D} + I_{\text{substrate}}} \tag{3}$$

In Figure 2c we show three data sets of C for 1L, 2L, and 3L MoS$_2$ recorded on different SiO$_2$ substrates with thicknesses 69, 121, and 278 nm. Notice that the range of the x-axis for the wavelength, going from approximately 400 to 850 nm, is limited by the microscope light source intensity that becomes negligible outside this range.

Knowing the refractive index of air, SiO$_2$, and Si (whose values are available in the literature) and the thicknesses of both the SiO$_2$ capping layer (see Figure S1, Supporting Information) and the TMDC layer, the only missing information to extract the optical contrast, and thus to reproduce the experimental data, is the refractive index of the TMDC. Expressions Equations (1–3) are thus used to determine the refractive

ADVANCED
SCIENCE NEWS
www.advancedsciencenews.com

ADVANCED
OPTICAL
MATERIALS
www.advopticalmat.de

index of the TMDC materials following the steps described below:

1) For a given TMDC material (MoS$_2$, MoSe$_2$, WS$_2$, or WSe$_2$) with a certain number of layers (1L, 2L, or 3L), we have a data set $C(\lambda,d_2)$, i.e., the optical contrast as a function of wavelength and SiO$_2$ thickness.
2) We select the first wavelength value ($\lambda = \lambda_1$).
3) For that wavelength value, a vector of optical contrast versus SiO$_2$ thickness can be evaluated, $C(\lambda = \lambda_1,d_2)$.
4) We then generate a $N \times N$ matrix with different pairs of n and κ values.
5) For each of the $N \times N$ pair of n and κ values the theoretical optical contrast versus SiO$_2$ thickness values is calculated using expressions.[1–3]
6) Among the $N \times N$ pairs of n and κ we select the one that minimizes the error with respect to the experimental data set. That n and κ determine the $\tilde{n}(\lambda = \lambda_1) = n - i \cdot \kappa$.
7) We select the next wavelength value ($\lambda = \lambda_2$) and we repeat the analysis starting from point 3.

Figure 3 shows examples of the best fits to the experimental optical contrast versus SiO$_2$ thickness obtained for 1L MoS$_2$ at selected wavelengths. The contrast between the SiO$_2$ and MoS$_2$ is a function of SiO$_2$ thickness at a particular wavelength, which depends on the interference conditions as described above in Equations (1–3). By fitting the experimental spectra, the complex refractive index $\tilde{n}(\lambda) = n - i \cdot \kappa$ can be obtained. The calculated complex refractive index $\tilde{n}(\lambda) = n - i \cdot \kappa$ for all wavelengths and different TMDCs is acquired after repeating these steps described above.

Figure 4 compiles the results following the protocol described above for 1L, 2L, and 3L MoS$_2$, MoSe$_2$, WS$_2$, and WSe$_2$ to determine their refractive index. Both the real and

imaginary parts of the refractive index show prominent features corresponding to excitons and are labeled according to the notation in the literature.[2,4,21] Overall, the locations of these peaks in κ correspond well to the exciton energies for 1L, 2L, and 3L TMDCs as the value of the imaginary refractive index is directly related to the absorbance of light in the material. The A exciton corresponds to the lowest energy direct transition between the valence and conduction band at the K point. The position of the A exciton blue shifts with a decreasing number of layers, which agrees with the fact that the direct bandgap energy increases in energy for thinner flakes.[3,21] Note that for some regions of the wavelengths, the uncertainty of the spectra is higher. Such uncertainty comes from the fact that the errors calculated with different values of n and κ are similar across these regions of wavelengths. This can generate some "artificial peaks" as seen in the case of 2L, 3L WS$_2$, where such peaks are inside the shaded areas and are thus regarded as artifacts. On the other hand, in the case of 1L WSe$_2$, an unexpected increase in κ above the wavelength of 750 nm is observed. This is likely caused by the detection limit of the spectrometer in the longer wavelength regime, which generates combinations of n and κ that seem to be absorptive in this particular case. A comparison with the literature values of the TMDCs refractive index is provided in Figures S5 and S6. In general, our monolayer results are in good agreement with the literature values obtained by different methods. Nonetheless, we find a systematic redshift of the excitonic features for the reported refractive index in Li and co-workers[8] as compared to our work for all materials, and also to other references in the case of MoS$_2$. Moreover, we find that the values of refractive index for a given wavelength show differences up to 20% in different reports even when calculated with the same technique. These discrepancies can originate in the material used or in the different details of the techniques.
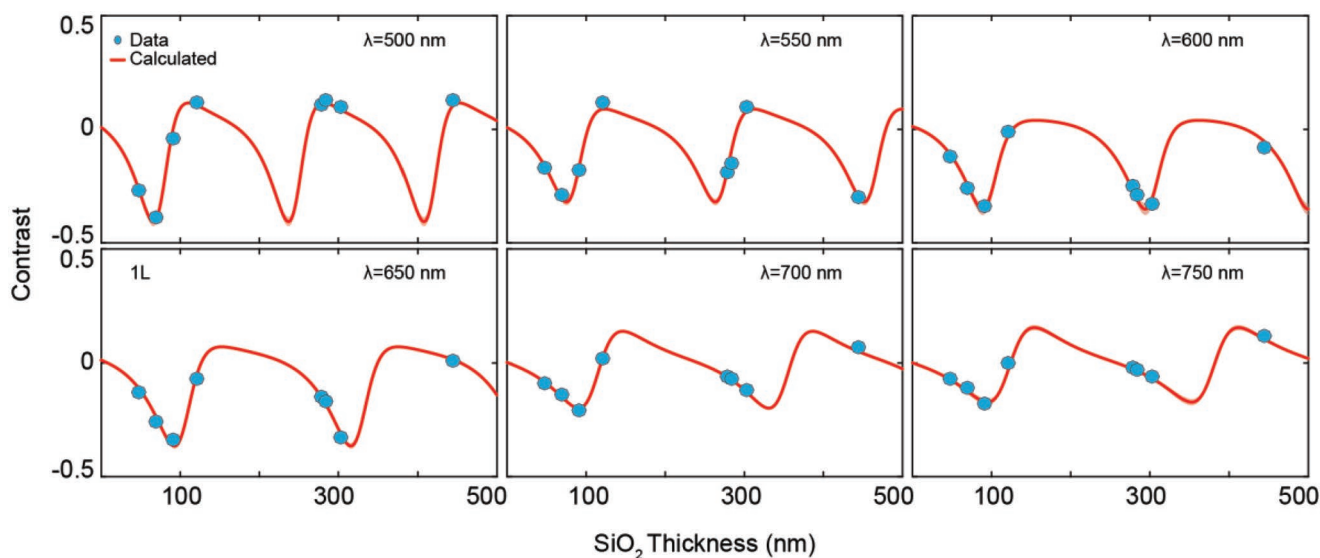

Figure 3. Optical contrast fitting of 1L MoS$_2$ for different SiO$_2$ thicknesses. The blue dots are the contrast data points for different thickness of SiO$_2$ at specific wavelengths; the red lines are fits with the Fresnel equations, where the error of n and κ is minimized. The uncertainty of the calculated contrast is shown as the shaded regions, which is small and not visible in some cases.
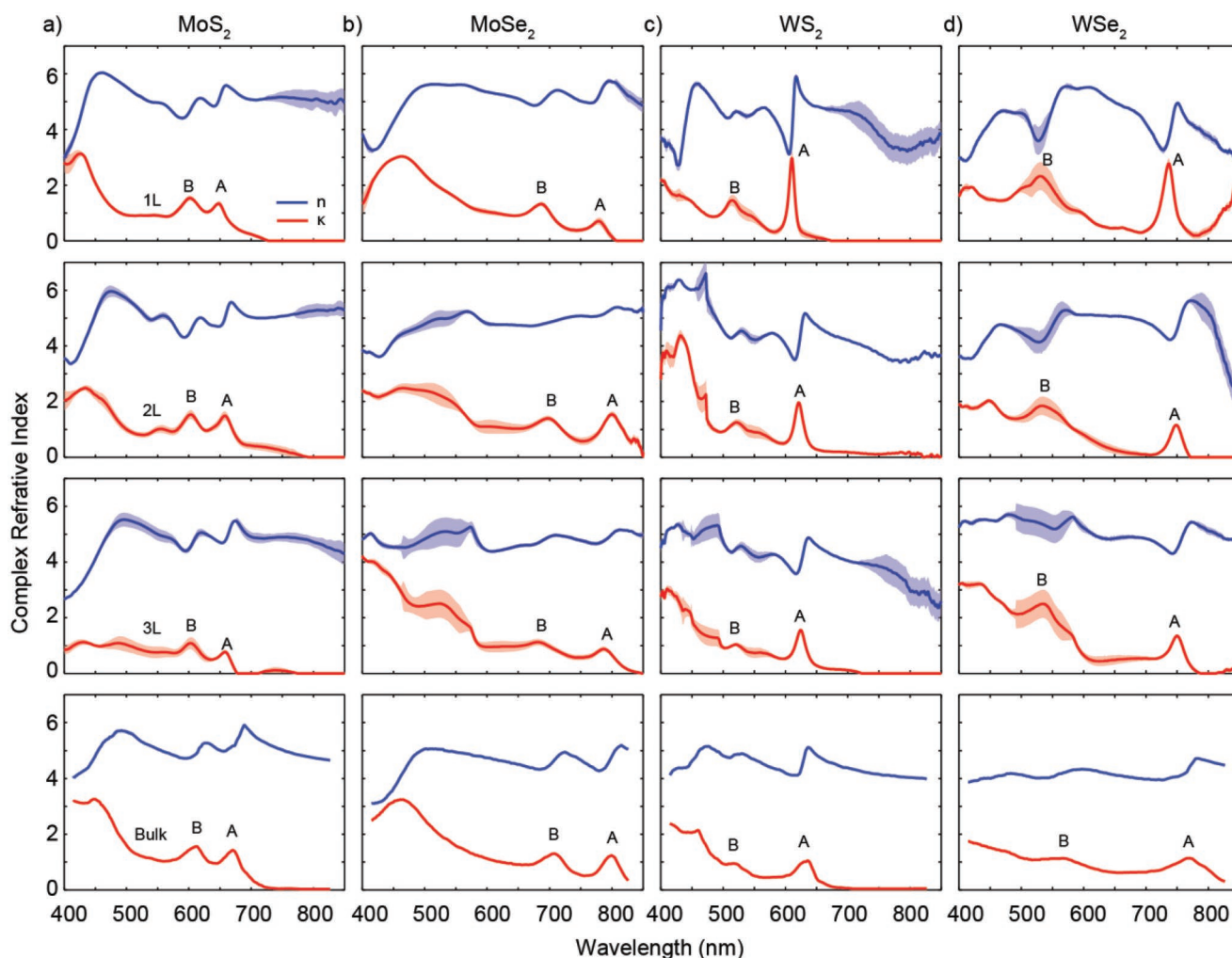
**ADVANCED
SCIENCE NEWS**

www.advancedsciencenews.com

**ADVANCED
OPTICAL
MATERIALS**

www.advopticalmat.de

Figure 4. Complex refractive index of TMDCs of different thicknesses. a–d) The refractive index of 1L, 2L, and 3L and bulk for MoS_2, $MoSe_2$, WS_2, and WSe_2, respectively. The bulk refractive index values are extracted from Beal and co-workers.[16,17] The uncertainty of the calculated refractive index is presented as the shaded area, and the labels A and B correspond to the A and B excitons described in the main text. The positions of peaks in κ agree well with the exciton peaks observed in reflectance or photoluminescence for the 1L–3L TMDCs.

We have systematically determined the complex refractive index for mechanically exfoliated 1L, 2L, and 3L MoS_2, $MoSe_2$, WS_2, and WSe_2 in the 400–850 nm range. We used the optical contrast of 1L, 2L, and 3L TMDCs on SiO_2/Si substrates with different SiO_2 thicknesses to calculate the refractive index with Fresnel law. We demonstrate that the refractive index of thin-film TMDCs converges to the bulk value as the thickness increases. A global blueshift of the excitonic features in the refractive index with respect to the bulk materials can be explained by a reduction of the quantum confinement in bulk compared to 1L–3L, and indicates that the refractive index is greatly influenced by the change of bandgap. The monolayer results are in good agreement with the literature, while the 2L and 3L measurements (not reported until now) show a strong exciton-dominant spectral response. Finally, the thickness-dependent refractive index that we report for Mo- and W-based TMDCs could be interesting to generate gradients in the refractive index for example to design novel guides for light at the nanoscale.

Experimental Section

Materials: We used naturally occurring molybdenite mineral rocks (Molly Hill mine, Quebec, Canada), synthetic $MoSe_2$ and WSe_2 crystals grown by the chemical vapor transport method, and WS_2 crystals grown by chemical vapor transport method at Tennessee Crystal Center.

Sample Fabrication: TMDCs flakes were first mechanically exfoliated from layered bulk single crystals with Nitto tape (Nitto SPV 224) and then transferred onto a Gelfilm (from Gelpak) substrate (a commercially available polydimethylsiloxane, PDMS, substrate). Prior to the transfer, the thickness of the flakes was determined by transmission mode optical microscopy, where we employ the transmittance spectrum and blue channel analysis. In the transmittance analysis, the light passing through the PDMS and flakes was analyzed by a spectrometer in the visible range (Thorlabs CCS200/M). By locating the absorbance peaks, the exciton energy was determined and compared with the literature for different thicknesses. The blue channel analysis exploited the strong thickness dependence of blue light transmittance in TMDCs. Optical images were taken and analyzed by using the blue channel in the RGB mode of the image. The obtained value $(1 - T)$ was then compared with the histogram shown in Figure 1d for thickness determination. After

thickness characterization, the flakes were dry-transferred onto SiO$_2$/Si substrates with different thicknesses.

Contrast Characterization: The optical contrast of the flakes on SiO$_2$/Si substrates was measured with a microreflectance set-up as described in Frisenda and co-workers.[19] A fiber-coupled Thorlabs spectrometer was connected to a Motic BAMET310 metallurgical microscope equipped with both transmission and epi-illumination halogen lamps. The reflection of the sample was used for the characterization of spectral contrast between the transferred flakes and SiO$_2$/Si substrates for different substrate thicknesses.

Supporting Information

Supporting Information is available from the Wiley Online Library or from the author.

Acknowledgements

Conflict of Interest

The authors declare no conflict of interest.

Keywords

[1] Q. H. Wang, K. Kalantar-Zadeh, A. Kis, J. N. Coleman, M. S. Strano, *Nat. Nanotechnol.* **2012**, *7*, 699.

[2] Y. Zhang, T.-R. Chang, B. Zhou, Y.-T. Cui, H. Yan, Z. Liu, F. Schmitt, J. Lee, R. Moore, Y. Chen, H. Lin, H.-T. Jeng, S.-K. Mo, Z. Hussain, A. Bansil, Z.-X. Shen, *Nat. Nanotechnol.* **2013**, *9*, 111.

[3] K. F. Mak, C. Lee, J. Hone, J. Shan, T. F. Heinz, *Phys. Rev. Lett.* **2010**, *105*, 2.

[4] A. Splendiani, L. Sun, Y. Zhang, T. Li, J. Kim, C. Y. Chim, G. Galli, F. Wang, *Nano Lett.* **2010**, *10*, 1271.

[5] F. H. L. Koppens, T. Mueller, P. Avouris, A. C. Ferrari, M. S. Vitiello, M. Polini, *Nat. Nanotechnol.* **2014**, *9*, 780.

[6] W. Choi, M. Y. Cho, A. Konar, J. H. Lee, G. B. Cha, S. C. Hong, S. Kim, J. Kim, D. Jena, J. Joo, S. Kim, *Adv. Mater.* **2012**, *24*, 5832.

[7] H. S. Lee, S. W. Min, Y. G. Chang, M. K. Park, T. Nam, H. Kim, J. H. Kim, S. Ryu, S. Im, *Nano Lett.* **2012**, *12*, 3695.

[8] Y. Li, A. Chernikov, X. Zhang, A. Rigosi, H. M. Hill, A. M. Van Der Zande, D. A. Chenet, E. M. Shih, J. Hone, T. F. Heinz, *Phys. Rev. B* **2014**, *90*, 1.

[9] C. Yim, M. O'Brien, N. McEvoy, S. Winters, I. Mirza, J. G. Lunney, G. S. Duesberg, *Appl. Phys. Lett.* **2014**, *104*, 103114.

[10] C.-C. Shen, Y.-T. Hsu, L.-J. Li, H.-L. Liu, *Appl. Phys. Express* **2013**, *6*, 125801.

[11] W. Li, A. G. Birdwell, M. Amani, R. A. Burke, X. Ling, Y. H. Lee, X. Liang, L. Peng, C. A. Richter, J. Kong, D. J. Gundlach, N. V. Nguyen, *Phys. Rev. B* **2014**, *90*, 1.

[12] H. Zhang, Y. Ma, Y. Wan, X. Rong, Z. Xie, W. Wang, L. Dai, *Sci. Rep.* **2015**, *5*, 8440.

[13] A. Castellanos-Gomez, N. Agraït, G. Rubio-Bollinger, *Appl. Phys. Lett.* **2010**, *96*, 213116.

[14] P. Gant, F. Ghasemi, D. Maeso, C. Munuera, E. López-Elvira, R. Frisenda, D. P. De Lara, G. Rubio-Bollinger, M. Garcia-Hernandez, A. Castellanos-Gomez, *Beilstein J. Nanotechnol.* **2017**, *8*, 2357.

[15] N. Papadopoulos, R. Frisenda, R. Biele, E. Flores, J.-R. Ares, S. Carlos, H. S. J. van der Zant, I. J. Ferrer, R. D'Agosta, A. Castellanos-Gomez, *Nanoscale* **2018**, *10*, 12424.

[16] A. R. Beal, W. Y. Liang, H. P. Hughes, *J. Phys. C: Solid State Phys.* **1976**, *9*, 2449.

[17] A. R. Beal, H. P. Hughes, *J. Phys. C: Solid State Phys.* **1979**, *12*, 881.

[18] Y. Yu, Y. Yu, Y. Cai, W. Li, A. Gurarslan, H. Peelaers, D. E. Aspnes, C. G. Van de Walle, N. V. Nguyen, Y.-W. Zhang, L. Cao, *Sci. Rep.* **2015**, *5*, 16996.

[19] R. Frisenda, Y. Niu, P. Gant, A. J. Molina-Mendoza, R. Schmidt, R. Bratschitsch, J. Liu, L. Fu, D. Dumcenco, A. Kis, D. P. De Lara, A. Castellanos-Gomez, *J. Phys. D: Appl. Phys.* **2017**, *50*, 074002.

[20] C. Janisch, H. Song, C. Zhou, Z. Lin, A. L. Elías, D. Ji, M. Terrones, Q. Gan, Z. Liu, in *Conf. Lasers Electro-Optics*, Washington DC, USA **2016**, p. SF2E.2.

[21] W. Zhao, Z. Ghorannevis, L. Chu, M. Toh, C. Kloc, P.-H. Tan, G. Eda, *Nano* **2013**, *7*, 791.

[22] A. Castellanos-Gomez, J. Quereda, H. P. van der Meulen, N. Agraït, G. Rubio-Bollinger, *Nanotechnology* **2016**, *27*, 115705.

[23] C. Lee, H. Yan, L. Brus, T. Heinz, J. Hone, S. Ryu, *ACS Nano* **2010**, *4*, 2695.

[24] K. P. Dhakal, D. L. Duong, J. Lee, H. Nam, M. Kim, M. Kan, Y. H. Lee, J. Kim, *Nanoscale* **2014**, *6*, 13028.

[25] Y. Niu, S. Gonzalez-Abad, R. Frisenda, P. Marauhn, M. Drüppel, P. Gant, R. Schmidt, N. S. Taghavi, D. Barcons, A. J. Molina-Mendoza, S. M. De Vasconcellos, R. Bratschitsch, D. P. De Lara, M. Rohlfing, A. Castellanos-Gomez, *Nanomaterials*, **2018**, *8*, 725.

[26] H. Li, J. Wu, X. Huang, G. Lu, J. Yang, X. Lu, Q. Xiong, H. Zhang, *ACS Nano* **2013**, *7*, 10344.

[27] A. Castellanos-Gomez, M. Buscema, R. Molenaar, V. Singh, L. Janssen, H. S. J. van der Zant, G. A. Steele, *2D Mater.* **2014**, *1*, 011002.

[28] R. Frisenda, E. Navarro-Moratalla, P. Gant, D. P. De Lara, P. Jarillo-Herrero, R. V. Gorbachev, A. Castellanos-Gomez, *Chem. Soc. Rev.* **2018**, *47*, 53.

[29] H. Zhang, Y. Ma, Y. Wan, X. Rong, Z. Xie, W. Wang, L. Dai, *Sci. Rep.* **2015**, *5*, 1.